ACS Infectious Diseases

Article

Screening and phenotypical characterization of Schistosoma mansoni histone deacetylase 8 (SmHDAC8) inhibitors as multi-stage antischistosomal agents

Fulvio Saccoccia, Margherita Brindisi, Roberto Gimmelli, Nicola Relitti, Alessandra Guidi, A. Prasanth Saraswati, Caterina Cavella, Simone Brogi, Giulia Chemi, stefania butini, Giuliana Papoff, Johanna Senger, Daniel Herp, Manfred Jung, Giuseppe Campiani, Sandra Gemma, and Giovina Ruberti

ACS Infect. Dis., **Just Accepted Manuscript** • DOI: 10.1021/acsinfecdis.9b00224 • Publication Date (Web): 29 Oct 2019

Just Accepted

is published by the American Chemical Society. 1155 Sixteenth Street N.W., Washington, DC 20036

Screening and phenotypical characterization of *Schistosoma mansoni* histone deacetylase 8 (*Sm*HDAC8) inhibitors as multi-stage anti-schistosomal agents

Fulvio Saccoccia,[a,^] Margherita Brindisi,[b,^] Roberto Gimmelli,[a] Nicola Relitti,[c] Alessandra Guidi,[a] A Prasanth Saraswati,[c] Caterina Cavella,[c] Simone Brogi,[c,d] Giulia Chemi,[c] Stefania Butini,[c] Giuliana Papoff,[a] Johanna Senger,[e] Daniel Herp,[e] Manfred Jung,[e] Giuseppe Campiani,[c,*] Sandra Gemma,[c,*] Giovina Ruberti [a,*]

[a]Institute of Biochemistry and Cell Biology (IBBC), National Research Council (CNR), Campus A. Buzzati-Traverso, via E. Ramarini 32, 00015 Monterotondo (Rome), Italy

[b]Department of Excellence of Pharmacy, University of Napoli Federico II, via D. Montesano 49, 80131 Naples, Italy

[c]Department of Excellence of Biotechnology, Chemistry and Pharmacy, University of Siena, via Aldo Moro 2, 53100, Siena, Italy

[d]Department of Pharmacy, University of Pisa, via Bonanno 6, 56126, Pisa, Italy

[e]Institute of Pharmaceutical Sciences, University of Freiburg, Albertstraße 25, 79104 Freiburg, Germany

*Corresponding authors:

campiani@unisi.it; gemma@unisi.it; giovina.ruberti@cnr.it

Keywords: *Schistosoma mansoni*, histone deacetylase inhibitors, *Sm*HDAC8, *h*HDAC8, screening, biological characterization

Schistosomiasis (also known as bilharzia) is a neglected tropical disease caused by platyhelminths of the genus *Schistosoma*. The disease is endemic in tropical and subtropical areas of the world where water is infested by the intermediate parasite host, the snail. More than 800 million people live in endemic areas and more than 200 million are infected and require treatment. Praziquantel (PZQ) is the drug of choice for schistosomiasis treatment and transmission control being safe and very effective against adult worms of all the clinically relevant *Schistosoma* species. Unfortunately, it is ineffective on immature, juvenile worms, therefore it does not prevent re-infection. Moreover, the risk of development and spread of drug resistance due to the wide use of a single drug in such a large population represents a serious threat. Therefore, research aimed to identifying novel drugs to be used alone or in combination with PZQ are needed. *Schistosoma mansoni* histone deacetylase 8 (*Sm*HDAC8) is a class I zinc-dependent HDAC which is abundantly expressed in all stages of its life cycle, thus representing an interesting target for drug discovery. Through virtual screening and phenotypical characterization of selected hits, we discovered two main chemical classes of compounds characterized by the presence of a hydroxamate-based metal binding group coupled to a spiroindoline or a tricyclic thieno[3,2-*b*]indole core as capping groups. Some of the compounds of both classes were deeply investigated and showed to impair viability of larval, juvenile, and adult schistosomes, to impact egg production *in vitro* and/or to induce morphological alterations of the adult schistosome reproductive systems. Noteworthy, all of them inhibit the recombinant form of *Sm*HDAC8 enzyme *in vitro*. Overall, we identified very interesting scaffolds paving the way to the development of effective anti-schistosomal agents.

Schistosomiasis, one of the most prevalent neglected parasitic diseases affecting more than 200 million people worldwide, mainly in tropical and sub-tropical areas, is caused by the

Platyhelminthes of the genus *Schistosoma*.[1] The pathology is due to eggs being trapped into host tissues once released by female worms into the circulation. To date, praziquantel (PZQ, **1**, Figure 1) is the only drug approved for the treatment of schistosomiasis, being very effective against adult worms of the most clinically relevant *Schistosoma* species (*S. mansoni*, *S. haematobium* and *S. japonicum*).[2] However, PZQ is poorly effective against the juvenile parasites and reinfection is common.[3-5] The increasing threat of drug-resistance coupled to the need for drugs with wider efficacy towards different parasite life cycle stages prompted the search for new druggable targets and compounds for the treatment of schistosomiasis.

Screening of compound libraries *in vitro* and *in vivo*, drug repurposing and target-based drug discovery have been used in order to identify novel compounds with anti-schistosomal activity. Promising compounds with different scaffolds have been discovered and could contribute to the development of new drugs (i.e. oxamniquine derivatives, biarylalkyl carboxylic acid derivatives (BACADs), arylmethylamino steroids (AASs), N,N´-diarylureas and analogues, thioredoxin glutathione reductase (TGR) Inhibitors, kinase inhibitors, cysteine protease inhibitors, 3-hydroxy-3-methyl-glutaryl-CoA (HMG-CoA) reductase inhibitors and schistosomal histone deacetylase (HDAC) inhibitors).[6,7]

HDACs have emerged as promising drug targets in many research areas, including parasitic diseases.[8,9] HDACs are Zn^{2+}- or NAD^{+}-dependent lysine deacetylases that modulate cell chromatin structure, transcription, and gene expression as well as several cytoplasmic signaling pathways.[10-13] *S. mansoni* HDAC8 (*Sm*HDAC8) is a class I zinc-dependent HDAC, which was demonstrated to be abundantly expressed in all *S. mansoni* life cycle stages; therefore it has been recently proposed as a promising target for drug discovery.[11,14] Noteworthy, the human homologue (*h*HDAC8) is poorly expressed in healthy cells, with a potential as a therapeutic target in cancer cells.[15] As a consequence, several efforts were spent in order to identify promising antiparasitic hits that may target *Sm*HDAC8. Recently

reported *Sm*HDAC8 inhibitors are depicted in Figure 1 (**2, 3**).[16-21] In the present paper, starting from structure-based virtual screening, we identified the effective compounds **4-12** (Figure 1). These were investigated in their ability to impair viability of *S. mansoni* larval stage (schistosomula), juvenile schistosomes, and adult pairs in addition to their impact on egg production and/or to induce alterations in the reproductive organs' morphology. The selected compounds demonstrated to inhibit recombinant form of *Sm*HDAC8 in the low micromolar range.

Results and Discussion

Virtual screening

We performed a structure-based virtual screening campaign based on a High Throughput Docking (HTD) approach as previously described[22-24] with the aim of identifying novel *Sm*HDAC8 inhibitors. The crystal structure of *Sm*HDAC8 (PDB ID: 4BZ7)[16] was employed to screen our in-house chemical library. This library is composed by ≈ 3000 compounds containing a variety of heterocyclic and peptidomimetic templates rationally designed for a broad range of biological targets, and is enriched with inhibitors of metallo-enzymes.[23,25-27] Our proprietary database was screened using Glide software[28] applying specific criteria based on the evaluation of Glide extra precision (XP) score followed by a rescoring using Glide standard precision (SP) scoring function. All the compounds showing a computational score ≤ -9.00 kcal/mol, computed on the scoring and rescoring procedure, were kept as potential *Sm*HDAC8 inhibitors. The protocol provided twenty-nine compounds that were selected to undergo biological screening. Remarkably, a number of compounds bearing metal-binding groups (MBG) and arising from medicinal chemistry projects focused on the development of anticancer agents, were retrieved.

Chemistry

Compounds **4** and **5** (Figure 1) were synthesized as previously described.[25] Compounds **6** and **7** were synthesized as described in Figure 2, panel A. The previous protocol was adapted to the synthesis of 2-arylderivatives **6** and **7.** Ketone intermediates **15a,b** were synthesized starting from the corresponding tosylhydrazone derivative **14** synthesized from **13** as reported.[29] Ketones **15a,b** underwent Fisher reaction with phenylhydrazine in the presence of concentrated sulfuric acid. The double bond of the resulting indolenines was reduced with sodium borohydride in methanol, and the secondary amines **16a,b** thus obtained were subjected to a reductive amination protocol with methyl 4-formylbenzoate. The resulting ester intermediates were converted to racemic hydroxamic acids **6** and **7** upon treatment with hydroxylamine hydrochloride.

Compounds **8-10** were prepared starting from cinnamic acid **17** as described in Figure 2, panel B. The 2-aryl-3,4-dihydro-2*H*-thieno[3,2-*b*]indole core was prepared according to a reported procedure.[30] Addition of triethylamine to a mixture of mercaptoacetic acid and cinnamic acid **17** in 1,4-dioxane yielded the 3-[(carboxymethyl)thio]-3-phenylpropanoic acid, which upon heating to 120 °C in the presence of acetic anhydride and sodium acetate, afforded the cyclic keto-derivative **18**. Intermediate **18** and the appropriate 4-halophenylhydrazine were suspended in ethanol and subjected to microwave irradiation to obtain tricyclic thienoindole derivatives **19a,b**. Intermediates **19a,b** were subjected to an alkylation reaction with methyl 4-(bromomethyl)benzoate in presence of potassium *tert*-butoxide giving the corresponding esters **20a,b**. Starting from **19b**, ester **21** was obtained through an alkylation reaction using methyl 5-(bromomethyl)thiophene-2-carboxylate (prepared as described in Scheme S1 of the Supporting Information). Esters **20a,b** and **21** were finally subjected to a reaction with hydroxylamine and potassium hydroxide to afford the final hydroxamic acids **8-10**.

The synthesis of **11** (Figure 2, panel C) was accomplished reacting *p*-toluenesulfonyl hydrazide **13** with acetone to obtain the tosylhydrazone intermediate **22**. This compound

was treated with 3-pyridinecarboxaldehyde in the presence of cesium carbonate to afford the ketone **23,** which was then used in the Fischer reaction with 4-methoxyphenylhydrazine to provide the indolenine intermediate. The double bond of this latter compound was reduced by catalytic hydrogenation and the corresponding amine **24** was subjected to a reductive amination procedure with methyl 4-formylbenzoate. The ester derivative obtained, was treated with hydroxylamine solution and potassium hydroxide to afford the final compound **11**.

Schistosomula assays for initial compounds screening

One of the major hurdles in structure-based drug design is the identification of enzyme inhibitors that, despite a fair potency against the target enzyme, are also characterized by high activity in whole cell or whole organisms, having suitable drug-like properties, such as cell penetration[26]. To address this issue, compounds from our virtual screening campaign, were screened using the ATP-based viability assay developed in our laboratory on *S. mansoni* larval stage (schistosomula).[31] A 60% viability reduction upon treatment at the concentration of 50 μM was set up as cut-off value together with DMSO (100% viability) and gambogic acid (0% viability) as negative and positive controls, respectively. Seven out of twenty-nine compounds, namely **4-10** showed to be effective *in vitro*, decreasing the schistosomula viability by 80-90% 72 h after treatment. Two more compounds, **11** and **12** showed to impact larvae viability to a lower extent, with a 35-40% reduction. Next, in order to calculate the $LC_{50,}$ dose-response curves were designed by treating schistosomula with each of the hits at concentrations ranging from 0.7 up to 100 μM. The LC_{50} of compounds 4-12 are reported in Figure 3, panel A, along with dose-response curves (Figure 3, panel B for the most structurally diverse and representative compounds **4**, **6**, **8**, **11** and Figure S1 for compounds **5**, **7**, **9**, **10**, and **12**).

This initial screening of compounds deriving from the virtually selected pool, was aimed at identifying promising hit compounds able to kill the larvae with a good potency. It is well

known that different stages of the schistosome life cycle have different susceptibility to drug actions;[32] therefore the activity of the most promising compounds was investigated against adult and juvenile *S. mansoni*.

Effects of the hit compounds on adult *S. mansoni* worm pair's viability

In order to investigate the effects of compounds active on schistosomula toward other parasite developmental stages, adult *S. mansoni* worm pairs were treated with the most promising compounds **4-12** both at 20 μM and 50 μM; their impact on parasite viability was monitored for seven days upon treatment. Viability of each schistosome was graded from 3 (normal) to 0 (severe effect) by assigning daily worm phenotype scores (plate-attachment, movement, color, gut peristalsis, tegument damage).[31] Six out of the nine compounds, namely **6** to **11** showed to markedly decrease the viability of treated worms at 50 μM. In particular, upon treatment with **9** viability dropped below 40% whereas with all others it was below 10% within the seven days (Figure 4). Vehicle-treated worms were always included in the assays and used for comparison. At 50 μM concentration, with the unique exception of compound **11**, the first 24 h showed to be critical, with the main drop on worm's viability exerted after the first day of treatment. Then, a slower decrease in viability was recorded. Treatment with **6** and **7** at the highest concentration showed to give the aforementioned immediate loss of viability, followed by a slower decrease in residual viability for the following six days until parasites death. The same compounds used at 20 μM, behaved differently, with **6** retaining a slightly higher potency than **7**; parasites treated with both compounds received an overall high score even though **6** appeared to interfere slightly more with the viability status. The initial viability drop was also observed after treatment with compound **10** at both concentrations. Treatment with both **8** and **10** at 50 μM resulted in worm death within five and seven days, respectively. On the other hand, compound **9** impacted viability to a much lesser extent and did not induce complete parasites death. All the effective compounds were also assayed on mammalian NIH-3T3 cells, by MTT assay, in a dose

response curve. Compound **7** was the most toxic (IC_{50} 2.37 μM ± 0.37 SEM), whereas compounds **6, 9-11** showed an IC_{50} around 10 μM and compound **8** had an IC_{50} in the high micromolar range (Figure 3, panel C).

Egg production impairment

Compounds **6-11,** showed to be the most effective in killing adult worms (viability less then 40% at day 7 upon treatment at 50 μM), were then evaluated for their impact on egg production *in vitro.* First, the highest sub-lethal concentration which ensured 100% viability and pairing was identified for each compound, hence, eggs of *in vitro* treated-worms were counted at 72 h and normalized to the number of couples. In particular, worm pairs were treated using the following concentrations for each selected compound: **6**, **7** and **11** were used at 10 μM, **8** at 20 μM, **9** at 30 μM, and **10** at 5 μM. The above conditions resulted in fully viable couples despite compounds **8, 9,** and **10** clearly showed reduced egg laying *in vitro* (Figure 5, panel A); compounds **8** and **9** treated samples also showed evident signs of egg damage (Figure 5, panel B). Worms treated with sub-lethal concentration of compounds **6** and **7** resulted in the presence of vitelline and germ cells with egg fragments in the culture medium. These were very abundant in compound **7**-treated samples, where damaged eggs were also detected (Figure 5, panel B). This turned our focus into assessing if any damage could be detected in the reproductive systems of the parasites.

Alterations of the reproductive systems of *S. mansoni* worm pairs treated with sub-lethal doses of selected compounds

Adult worm couples were analyzed by means of carmine red staining followed by confocal laser scanning microscopy (CLSM). Sub-lethal doses of compounds were chosen to preserve the overall parasite viability and pairing. For each compound, three to five couples were analyzed and images of ootype, ovary, vitellarium, testis and parenchyma recorded. All observations were compared with the morphology as well as organs and tissues organization of control (DMSO) worms (Figure 6 and Figure S2, S3).

Worm pairs treated with compound **6** (10 μM) showed either an empty ootype or vitelline cells and oocytes accumulation (Figure 6). In three out of four samples no properly, developed eggs were detected. The overall morphology of ovary and vitellarium was preserved in compound **6**-treated females however cell degeneration was observed in the ovary, especially in the immature compartment, and in the vitellarium in all samples (Figure 6). Treatment with compound **6** resulted also in an increase in the number of sperm cells in testis and relative seminal vesicle (Figure 6). No alterations in the sub-muscle layers were detected. Pairs treated with compound **7** (10 μM) showed phenotypic alterations similar to those of compound **6**-treated schistosomes (Figure S2). Interestingly, treatment with compound **6** and **7** did not impact the number of eggs layed *in vitro,* nevertheless egg-shell fragments, vitellocytes, oocytes and sperms were detected in the medium and some eggs were damaged in compound **7**-treated samples (Figure 5B). These observations, along with the CSLM analysis, suggest the possibility that the eggs were properly released within the first 48 h; after that time a possible drop in egg production might occur due to reproductive organs damage.

Regarding compound **8** (20 μM), the ootype was found empty in four out of five females (one contained only vitelline cell aggregates) (Figure 6); the ovary morphology was unaffected, even though cellular degeneration, in particular in the immature compartment, was observed. Moreover, black spots (alterations previously observed upon treatment with other synthetic compounds[33,34]) were detected in a large number of mature oocytes (Figure 6). The vitelline cells appeared to be irregular and disordered and dark areas resembling hole-like structures within the vitellarium were also detected in all samples, likely due to lipid aggregation in vitelline cells (Figure 6).[35] Within the seminal duct and seminal vesicle of three male parasites an accumulation of sperm cells was found (Figure 6), whereas one specimen showed a collapsed seminal vesicle and in one male no clear accumulation of spermatozoa, with respect to control worms, was observed. Moreover, a generalized

damage for the male parenchymal tissue with numerous unstained dark areas was present (Figure 6).

Couples treatment with compound **9** (20 μM) was not associated to alterations within the vitellarium and ovary; yet the ootype was empty in two out of three samples (Figure S3a); as for worms treated with compound **8** (Figure 6). It is worth noting that control worms (DMSO-treated) displayed eggs within the ootype in almost all the specimens investigated. On the contrary, alterations similar to the ones described for compound **8**, were detected in some of the worms treated with compound **9** at slightly higher concentrations (30 μM), namely: cell degeneration in the ovary in half of the samples; sperms accumulation in one out of the three samples in testis; numerous unstained, dark, hole-like areas in the vitellarium (all samples) and in the parenchyma in two out of three (Figure S3b). These observations, along with the diminished egg counts (Figure 5), lead us to hypothesize that the reproductive systems are the main site of action of compounds **8** and **9**.

The small but significant decrease in egg-laying detected in worm pairs treated with compound **10** at 5 μM (Figure 5A) was not associated to CSLM morphological alterations within the reproductive organs in 3 samples (Figure S2).

Effect of selected compounds on male juvenile worms

All compounds, effective on adult parasites, were also tested against juvenile schistosomes (4-week-old parasites) poorly sensitive to PZQ.[32] Male parasites were subjected to the same treatment conditions as for adult pairs, namely 20 and 50 μM of the selected compounds for up to 7 days. At these conditions, only compound **11** did not show any striking effect, whereas the remaining compounds, especially at 50 μM, showed a strong lethal phenotype already three days after treatment, with parasites death occurring 5 days post treatment (Figure 7). In addition, **6** and **7** exerted the same lethal effect also using low compound concentrations, resulting more active on juvenile parasites than on the adult ones (Figure 4). Noteworthy treatment with both concentrations showed an initial drop in parasite's

viability as observed for adult worms (50 μM). This implies that almost all the effects in terms of viability and phenotypic changes occurred within the first 24 h, after which viability slowly decreases throughout. In general, the overall sensitivity to the compounds is shared between adult and juvenile stages with the latter one showing a higher susceptibility, with the exception represented by compounds **9** and **11** having major activity on adults (Figure 4). Taken together, these data suggest that compounds **8, 9** and **10**, sharing a thienoindolyl core, not only have similar effects in killing all the developmental parasite stages of the definitive host (schistosomula, juvenile, and adult schistosomes) but were also able to impact egg-laying at sub-lethal doses. Compound **6** showed to be very effective in killing adult and juvenile worms at 20 μM; its isomer **7** was less potent on adult parasites. Compounds **8** and **9** were not able to kill the parasite at lower concentrations; rather, their main action was exerted by impairing the egg-laying.

Activity of hit compounds on recombinant *Sm*HDAC8 and docking studies of selected inhibitors with *Sm*HDAC8

In order to investigate the mechanism of action of molecules **4-12,** *Sm*HDAC8 enzymatic assays were performed *in vitro*. A recombinant form of the *Sm*HDAC8 was produced in *E. coli* and assayed for its residual activity upon pre-incubation with each of the selected compounds. The activity assays were performed by using commercially available fluorescence-based kit, and residual activity of the enzyme was evaluated with respect to the untreated enzyme. The residual activity was also measured for the *human* HDAC8 (*h*HDAC8) treated with the same compounds. An initial screening, performed at 50 μM for the whole set of selected compounds, demonstrated that only compounds **6-11** were inhibitors of both homologue forms. Hence, a dose-response curve was designed for the same compounds and the alleged IC_{50} values were calculated; the results are shown in Figure 8. The data indicate that compounds **6-11** are inhibitors of both *Sm*HDAC8 and *h*HDAC8 enzymes, with the whole set of IC_{50} values in the low micromolar range. Since

hHDAC8 belongs to class I histone deacetylases, to further characterize the new HDAC inhibitors, we tested compounds **6**-**11** against HDAC1, a nuclear enzyme isoform that belongs to the same class. Two- to three-fold lower IC_{50} values were recorded on *h*HDAC1 for compounds **6**, **8**, and **11**, while similar values were observed for inhibitors **7** and **9.** Gratifyingly, compound **10** showed only 44% *h*HDAC1 inhibition even at 50 μM (Figure 8).

In order to gain insights into the binding mode of compounds **6-11** we performed *Sm*HDAC8 docking experiments. All the presented compounds reported a docking score below -9.00 kcal/mol that represents the minimal requirement for selecting molecules in our virtual screening procedure (see Experimental section for further details). In particular, in Figure 9 the poses of the compounds most effective on schistosomes are reported. They belonging to two structural templates, namely indolines such as compound **6** (Figure 9 A, B for *R*- and *S*-enantiomers, respectively) and thieno[3,2-*b*]indoles as for inhibitor **10** (Figure 9 C,D for *R*- and *S*-enantiomers, respectively). Binding poses of compounds **7-9** are reported in the Supporting Information (Figure S4). For each compound, the potential coordination bond is established by the carbonyl moiety of the hydroxamic portion of the molecule with Zn^{2+} through a monodentate coordination. The *R*-enantiomer of **6** (panel A) was differently accommodated as compared to the corresponding *S*-enantiomer. In particular, the phenyl ring of the pendant benzyl moiety of the *R*-**6** can form two different π-π stackings with F151 and H188 of the enzyme. Two additional stackings, with H292 and with F216 are also established through the chlorophenyl moiety and the indoline ring. In terms of polar contacts, the *R*-enantiomer of compound **6** can form an H-bond with G150, as depicted in Figure 6 and a salt bridge through its protonated methylpiperidine with D100. The main difference in the binding mode of the *S*-enantiomer of compound **6** is represented by the different accommodation of the cap group in the binding site, which now establishes a cation-π stacking with H292 through its protonated piperidine N-atom, while the central portion of the molecule maintains the same contacts.

On the other hand, the *R*- and *S*- enantiomers of **10** were similarly accommodated inside the binding site. The MBG of the two enantiomers can form an H-bond with G150 through the NH moiety of the hydroxamic acid and another H-bond with Y341 through the carbonyl moiety of the MBG. The thiophene ring establishes two π-π stackings with F151 and H188, while the two phenyl rings of the cap group can establish two π-π stacking with F215 and F216 for *R*-enantiomer, while the *S*-enantiomer lack the stacking with F215, due to its different conformation with respect to *R*-enantiomer (Figure 9 panel D).

In addition, the aforementioned compounds were evaluated for their potential capability to behave as pan-assay interference compounds (PAINS), namely compounds that frequently give positive results in screening campaigns due to nonspecific reactions with several biological targets.[36] This calculation was performed by means of FAFDrugs4.0 (http://www.fafdrugs4.mti.univ-paris-diderot.fr/ access date December 2018).[37] Remarkably, the compounds filtered for PAINS indicated that none of them was labeled as potential "frequent hitter". For compound **11** the software highlighted the presence of the methoxydialkylaniline as a low-risk structural alert with a number of occurrences below the threshold. Due to this low risk, compound **11** was retained for evaluation of its biological activity.

HDAC inhibitors treatment causes histones hyperacetylation

In order to investigate the effects of the selected compounds on HDACs activity, acetylation of lysine residues within histone proteins was evaluated. Worm pairs were treated with sub-lethal doses (20 μM) of selected compounds; after 72 h, histone-enriched fractions of parasite lysates have been subjected to SDS-PAGE and western blot analysis (Figure 10). Treatment with the pan inhibitor TSA (1 μM) was used as positive control of histones hyperacetylation. A strong signal was detected for samples treated with compounds **8-10** whereas no changes in acetylation signal was associated to compounds **6**, **7** and **11** parasites-treatment (Figure 10).

It is worth noting that schistosomes treated with compounds **6** and **7** did not show any detectable increase in histones acetylation, even though they behave as inhibitors of recombinant *Sm*HDAC8 activity *in vitro*. However, it has been recently reported that HDAC8 can also deacetylate non-histone substrates[12,38,39] and several nuclear and cytoplasmic acetylated proteins have been also identified in *Schistosoma*.[40]

Conclusions

We deepen the investigation of the biological effects associated to treatment of *Schistosoma* with two main chemical classes of HDAC inhibitors characterized by the presence of a hydroxamate-based MBG coupled to a (spiro)indoline or a tricyclic thieno[3,2-*b*]indole core as capping groups (compounds **4-7** and **8-10**, respectively). Compounds of both classes were shown to impair the viability of multiple life cycle stages of *S. mansoni* (schistosomula, juvenile and adult parasites); compounds **8-10** also decrease egg-laying *in vitro* and treatment with compounds **6-9** has been associated to morphological alteration in the reproductive organs of adult pairs. Compounds **6-11** demonstrated to inhibit the enzymatic activity of recombinant form of *Sm*HDAC8 in the low micromolar range. Based on these results, following studies should be aimed at optimizing potency and selectivity of the new (hetero)arylhydroxamate-based molecules in order to proceed to their evaluation in murine models of infection. Moreover, based on the innovative mode of action of *Sm*HDAC8 inhibitors, with respect to currently available drugs, combination therapy should be considered early in compounds optimization phase as a strategy to improve efficacy on multiple developmental stages including juvenile schistosomes, and to avoid selection of drug-resistant parasites.

Experimental Section

Chemistry

General procedures. Starting materials and solvents were purchased from commercial suppliers and used without further purification. Reaction progress was monitored by TLC using silica gel 60 F254 (0.040-0.063 mm) with detection by UV. Silica gel 60 (0.040-0.063 mm) was used for column chromatography ^{1}H NMR and ^{13}C NMR spectra were recorded on a Varian 300 MHz, or a Bruker 400 MHz spectrometer using the residual signal of the deuterated solvent as internal standard. Splitting patterns are described as singlet (s), doublet (d), triplet (t), quartet (q), and broad (br); the value of chemical shifts (™) are given in ppm and coupling constants (*J*) in Hertz (Hz). Mass spectra were recorded utilizing electron spray ionization (ESI) Agilent 1100 Series LC/MSD spectrometer. Melting points were determined using a Büchi® Melting point B-540. Yields refer to purified products and are not optimized. All moisture-sensitive reactions were performed under argon atmosphere using oven-dried glassware and anhydrous solvents. All compounds that were tested in the biological assays were analyzed by combustion analysis (CHN) to confirm the purity > 95%.

Computational Details

Database and protein preparation and High Throughput Docking protocol. Our proprietary database was built in Maestro suite[41]. All the structures were minimized by means of MacroModel[42] with OPLSAA_2005.[43] The GB/SA model was used for simulating the solvent effect. PRCG method (10000 maximum iterations and 0.001 gradient convergence threshold) was employed. Compounds were then submitted to LigPrep program[44] producing a possible ionization state taking also into account all enantiomers and tautomers at pH 7.4 ± 0.2.

The three dimensional structure of *Sm*HDAC8 was taken from the PDB database (PDB ID: 4BZ7, Crystal structure of *Sm*HDAC8 complexed with M344, DOI: 10.2210/pdb4BZ7/pdb) and submitted to Protein Preparation Wizard protocol implemented in Maestro suite 2015 for obtaining a suitable protein structure for the screening protocol.[22,23] Water molecules and compounds used in the crystallization process were removed maintaining the Zn^{2+} ion and

the ligand M344. After the preparation protocol, the refined protein was used in HTD as reported in the next paragraph.

The HTD protocol was carried out employing Glide software[45] implemented in Maestro[46] suite using the database and the protein prepared as above-mentioned. Energy grid was prepared using default value of protein atom scaling factor (1.0 Å) within a cubic box centered on the crystallized inhibitor M344. After grid generation with the introduction of metal constrains[25], the ligands were docked into the enzyme. The number of poses entered to post-docking minimization was set to 50. In order to select the most promising compounds from our library, we used extra XP scoring function, coupled with a rescore procedure employing SP scoring function, applying a score cutoff of -9.00 kcal/mol.

Considering that our in-house database contains compounds with one or more stereogenic center, an additional criterion for molecules selection was that the enantiomers of a molecule must have a docking score below -9.00 kcal/mol. The assessment for potential Pan Assay Interference Compounds (PAINS) in the set of selected molecules was conducted by means of FAFDrugs4 (http://www. fafdrugs4.mti.univ-paris-diderot.fr/ access date December 2018).[36,37]

Schistosoma mansoni studies

Reagents. Dimethyl sulfoxide (DMSO), percoll, Nonidet P-40 (NP40), foetal bovine serum (FBS), thimerosal, gambogic acid, trichostatin A (TSA), bovine serum albumin (BSA), carmine-red and Canada balsam, thrombin from bovine plasma, protease inhibitor cocktail, DNase, were purchased from Sigma-Aldrich (Saint Louis, USA) and talon superflow histidine-tagged protein purification resin from GE Healthcare Life Sciences (Marlborough, USA); CellTiter-Glo (CTG) reagent from Promega (Madison, USA); Dulbecco-Modified Eagle's Medium (DMEM) with or without phenol red, HEPES, L-glutamine from Lonza (Basel, Switzerland); Trizol reagent, glycogen, RNA grade, T4 DNA Ligase, SuperScript™ III One-Step RT-PCR System with Platinum™ Taq High Fidelity DNA Polymerase, antibiotic-

antimycotic reagent (100×) from Thermo Fisher Scientific (Waltham, USA); the primary monoclonal anti-α-tubulin antibody (DM1A) from Sigma-Aldrich; the anti-acetylated-lysine (Ac-K2-100) from Cell Signaling Technology (Danvers, USA); the goat anti-mouse and anti-rabbit IgG (H+L)-horseradish peroxidase secondary antibodies from Bio-Rad Laboratories (Hercules, USA). Fluor De Lys HDAC8 Fluorimetric Drug Discovery Kit (BML-AK518) was from Enzo Lifescience (Farmingdale, USA), in the form of the BML-AK518 fluorimetric drug discovery kit.

***Sm*HDAC8 cloning.** Total RNA was extracted from 8-10 adult *S. mansoni* worms washed 3 times in 1.0 mL PBS resuspended in Trizol reagent (100 µL), flash frozen in liquid nitrogen and stored at −80°C for 1 h. During thawing, samples were homogenized with disposable pellet pestles served by cordless motor. Next, Trizol reagent was added up to 500 µL and samples extracted with 200 µL of chloroform-isoamyl alcohol mix (24:1). The aqueous phase was then transferred to a new 1.5 mL microfuge tube and RNA was precipitated with 250 µL of 2-propanol. RNA was further purified by two washes in 75% ethanol and pellet dried at room temperature was resuspended in fresh milliQ water. The full-length cDNA for *Sm*HDAC8[14] was PCR amplified with the oligonucleotides GR581 5'-CCCCCCATGGGATCTGTTGGGATCGTTTATGG-3' and GR583 5'-CCCCGAGCTCCATACCAGTTAAATTATATAATTG-3' and the SuperScript™ III one-step RT-PCR system. Next, the PCR product was purified and cloned between the NcoI and SacI sites of the pET-52b(+) plasmid encoding a C-terminal thrombin cleavage site followed by a His-tag. The recombinant plasmid was checked by nucleotide sequencing (Eurofins Genomics service). Overexpression of the His-tagged *Sm*HDAC8 was carried out in *E. coli* BL21(DE3) cells.

***Sm*HDAC8 expression in *E. coli* and purification.** The recombinant enzyme was produced accordingly with Marek et al.[47] with minor changes in the purification procedure. Briefly, freshly transformed *E. coli* BL21 (DE3) cells were spread on a LB agar plate

containing 100 μg/mL ampicillin and the bacteria film grown on the plate was resuspended and grown up to 20h in sterile Terrific Broth medium containing ampicillin, 0.17 M KH_2PO_4 and 0.72 M K_2HPO_4. Then, 500 μM IPTG and 100 μM $ZnCl_2$ were added to the culture in order to induce expression of the recombinant His-tagged protein. After 1 h, the *E coli* cells were harvested and the bacterial pellet resuspended in ice-cold purification buffer A (50 mM Tris, pH 8.0, 150 mM KCl, protease inhibitor cocktail, and 10 μg/mL DNase). After the lysis, the suspension was centrifuged at 28000 x g. From this point ahead, all of the purification procedure was conducted at 4°C. Major modifications in the already published procedure were as follows. For the protein purification, the supernatant was incubated 1 h in a glass flask containing 0.4 mL/L of Talon superflow affinity resin, previously equilibrated in buffer A. The resin was then loaded into a disposable plastic column and twashed with 150 mL of buffer A. Then, 60 U of thrombin in 6 mL of buffer A were added to the resin and left to incubate up to 16 h under shaking in order to release the protein. The resin was loaded into disposable plastic column and the eluate was collected followed by one or more washing step. The fractions before and after the thrombin cleavage were analyzed by 12% SDS-PAGE and those containing only the cleaved protein were pooled together and loaded into a pre-equilibrated (with buffer A) 1 mL HiTrap Q FF column. Elution was achieved by a step-wise gradient with increasing concentration of KCl (from 50 mM up to 600 mM) in 50 mM Tris, pH 8.0. Purity was were assessed by means of 12% SDS-PAGE. Usually *Sm*HDAC8 eluted between 250 mM and 450 mM KCl. The fractions containing the purified protein were pooled and diafiltrated 3 to 4 times against buffer B, 10 mM Tris, pH 8.0, 50 mM KCl, 2 mM DTT, using AMICON ULTRA 30 KDa MWCO and concentrated up to 2.5 mg/mL. The purified protein was then used within few days from the purification, in order to minimize unfolding events and/or metal leaking, otherwise a decrease in its activity was observed.

Activity and inhibition assay of recombinant form of human and *S. mansoni* HDAC8. Recombinant human HDAC8 was an item of the Fluor de Lys HDAC8 fluorimetric drug

discovery kit (Enzo Life Sciences, BML-AK518). Inhibition assays were performed as already described in previous publications[16,47,48] with minor modifications. Increasing concentrations of selected compounds were used in order to draw scattered curves by which IC_{50} value for each compound could be inferred with respect to human and *S. mansoni* enzymes. DMSO concentration was kept constant to 0.5% and for each compound, a control curve (enzymes incubated with DMSO only) was added. To keep safe from the possibility of a slow-binding interaction between the inhibitor and the target, each enzyme was pre-incubated with the selected compounds 15 minutes before substrate addition to the mixture. Fluor de Lys Substrate was used at 50 μM. Then, compounds, substrate and enzymes (1.7 μM SmHDAC8 or 1 μM for hHDAC8) were incubated and the reaction left to proceed for 1 h at 30°C; subsequently, 2 μM TSA within 50 μl of 1x Developer II was added and the mixture was further incubated for 1 h at 30°C to quench the reaction. Fluorescence was measured in a plate reader (Varioskan Lux, Thermofisher Scientifica) with excitation at λ = 370 nm and emission at λ = 450 nm. IC_{50} was obtained after non-linear regression curve fit performed by means of GNU/Octave, according to a generalized form of a dose-response curve equation, as reported by Copeland (2000; eq 8.25, p. 287 in the original text):

(1)

$$y = \frac{y_{max} - y_{min}}{1 + \left(\frac{[I]}{IC_{50}}\right)} + y_{min}$$

where y is the residual activity of the enzyme in the presence of inhibitor at concentration [I]; y_{max} is the maximum observed value for the enzyme at zero inhibitor concentration; y_{min} is the minimum observed value for the enzyme at the highest inhibitor concentration. The model did fit three parameters, IC_{50}, y_{max}, y_{min}, while assuming that the dose response curves has a Hill slope of -1.0.

HDAC1 assay. OptiPlate-96 black microplates (Perkin–Elmer) were employed with an assay volume of 60 μL. Human recombinant HDAC1 (BPS Bioscience, Catalog #: 50051)

was diluted in incubation buffer (50 mM Tris-HCl, pH 8.0, 137 mM NaCl, 2.7 mM KCl, 1 mM $MgCl_2$ and 1 mg/mL BSA). A total of 52 µL of this dilution were incubated with 3 µL of different concentrations of inhibitors in DMSO and 5 µL of the fluorogenic substrate ZMAL (Z-(Ac)Lys-AMC)[48,49] (126 µM) at 37°C. After 90 min incubation time, 60 µL of the stop solution (33 µM Trichostatin A and 6 mg/mL trypsin in trypsin buffer [Tris-HCl 50 mM, pH 8.0, NaCl 100 mM]), were added. After a following incubation at 37°C for 30 min, the fluorescence was measured on a BMG LABTECH POLARstar OPTIMA plate reader (BMG Labtechnologies, Germany) with an excitation wavelength of 390 nm and an emission wavelength of 460 nm [54,76].[49,50,51]

Western blot analysis. Ten adult pairs were treated with selected HDAC inhibitors for 72 h. Parasites were processed by using a modified version of Dubois et al.[52] protocol as previously described.[34] Samples were analyzed by 15% SDS-PAGE and immunoblotting using α-tubulin DM1A (1:5000) or α-acetylated-lysine (1:4000) antibodies according to manufacturer's instructions. A Chemidoc XRS Bio-Rad with a chemi-luminescent camera and ImageLab 4.0 software were used for acquisition of images. Each western blot analysis was calibrated by Ponceau-staining.

Ethics statement. Animal work was approved by the National Research Council, Institute of Cell Biology and Neurobiology animal welfare committee (OPBA) and by the competent authorities of the Italian Ministry of Health, DGSAF, Rome (authorization no. 25/2014-PR and no. 336/2018-PR). All experiments were conducted in respect to the 3R rules according to the ethical and safety rules and guidelines for the use of animals in biomedical research provided by the relevant Italian law and European Union Directive (Italian Legislative Decree 26/2014 and 2010/63/EU) and the international guiding principles for biomedical research involving animals (Council for the International Organizations of Medical Sciences, Geneva, Switzerland).

Maintenance of the *S. mansoni* life-cycle. A Puerto Rican strain of *S. mansoni* was maintained by cycling within albino *Biomphalaria glabrata*, as the intermediate host, and ICR (CD-1) outbred female mice as the definitive host as previously described.[31] Briefly, 2 to 3 months old-female mice (purchased from Envigo, Udine, Italy) were housed with the following conditions: 22 °C, 65% relative humidity, 12/12 h light/dark photocycle, standard food and water *ad libitum*. Then, they were infected with 200-250 single sex or double sex *S. mansoni* cercariae by the tail immersion technique. Juvenile (single sex) and adult parasites (double sex) were recovered from mice 4 or 8 weeks after infection by reversed perfusion of the hepatic portal system and mesenteric veins.

Schistosomula viability assay. Schistosomula were obtained by mechanical transformation of cecariae and percoll gradient. This stem from an optimized version of the protocol of Brink et al.[53] previously described by Protasio et al.[54] and adapted in our laboratory.[31] The viability assay was performed as already described[31] with minor modification. In brief, the schistosomula (150-200/wells) were incubated in DMEM medium (w/o phenol red) with compounds dissolved in DMSO for 72 hours, 37°C in 5% CO_2, in 96-well black plates. Then 50 µL of CellTiterGLO reagent (CTG) was added to each well and relative luminescence units (RLU) signal was recorded after 30 minutes with Varioskan Lux. Data analysis was achieved using GraphPad Prism v 7.0 software and IC50 was obtained after non-linear regression curve fitting performed according to log (inhibitor) vs. normalized response with variable slope curve model.

Viability assays on adult and juvenile worms and egg counts. For juvenile and adult worm assays, 10 juvenile worms or 5 adult pairs were incubated with selected compounds in 3 ml DMEM complete medium. For each compound, three experiments were carried out and compounds were given to parasites only once without medium addition and/or replacement. DMSO (vehicle) treated worms were used as control frame. Viability was monitored daily under a Leica MZ12 stereomicroscope for 7 days and scores assigned, as

previously reported.[31] In particular the following phenotype scoring criteria were adopted: 3, plate-attached, good movements, clear; 2, slower or diminished movements, darkening, minor tegumental damage; 1, movements heavily lowered, darkening, tegument heavily damaged; 0, dead, lack of any movement. For each sample the total score was determined by the ratio of the sum of worm scores for the total number of worms. Vehicle-treated samples were always included in the assays. Three days upon compound treatment, the number of eggs laid *in vitro* by worm couples was counted using an inverted Leica DM IL microscope (Leica Microsystems, Wetzlar, Germany) with a gridded-plate as supporting tool.

Confocal microscopy analysis. Carmine red staining was performed as previously described.[35] Images were acquired on an Olympus FV1200 confocal laser scanning microscope using a UplanFLN 40x immersion oil lens (NA = 1.30) with optical pinhole at 1 AU and a multiline argon laser focused. Excitation was at 488 nm and fluorescence was recovered in the range 500 nm to 700 nm. Images were collected as single stack.

Ancillary Information

Supporting Information

The Supporting Information is available free of charge on the ACS Publications website at DOI:

Scheme S1, Figure S1, Figure S2, Figure S3, Molecular Docking for compound **7** and **8,** Figure S4, Chemistry.

Author Information

Corresponding Authors

G. Campiani, Email: campiani@unisi.it; S. Gemma, Email: gemma@unisi.it; G. Ruberti, Email: giovina.ruberti@cnr.it

Author contribution

^F.S. and M.B. contributed equally to this work

Acknowledgments

This work was supported by Ministero dell'Istruzione, dell' Università e della Ricerca (MIUR) (PRIN Project 20154JRJPP to G.C. and G.R.), by the CNR (National Research Council)-CNCCS (Collezione Nazionale di Composti Chimici e Centro di screening) "Rare, Neglected and Poverty Related Diseases - Schistodiscovery Project" (DSB.AD011.001.003 to G.R.), and the Deutsche Forschungsgemeinschaft (DFG, Ju295/13.1). A special thanks to Stefania Colantoni for mouse husbandry and Pierluigi Palozzo for dishwashing lab technical support.

Abbreviations used

PZQ, Praziquantel; HDAC, Histone deacetylase; BACAD, biarylalkyl carboxylic acid derivative; AAS, arylmethylamino steroid; TGR, thioredoxin glutathione reductase; HMG-CoA, 3-hydroxy-3-methyl-glutaryl-CoA; HTD, High Throughput Docking; MBG, metal-binding group; CSLM, laser scanning microscopy; PAINS, pan-assay interference compound; ESI, electron spray ionization; DMSO, Dimethyl sulfoxide; RLU, relative luminescence units.

References

(1) World Health Organization, 2019. Schistosomiasis. https://www.who.int/schistosomiasis/en/ (07/01/2019).

(2) Cioli, D.; Pica-Mattoccia, L.; Basso, A.; Guidi, A. (2014) Schistosomiasis control: praziquantel forever? *Mol. Biochem. Parasitol.* 195, 23-29.

(3) da Silva, V. B. R.; Campos, B.; de Oliveira, J. F.; Decout, J. L.; do Carmo Alves de Lima, M. (2017) Medicinal chemistry of antischistosomal drugs: praziquantel and oxamniquine. *Bioorg. Med.Chem.* 25, 3259-3277.

(4) Siqueira, L. D. P.; Fontes, D. A. F.; Aguilera, C. S. B.; Timoteo, T. R. R.; Angelos, M. A.; Silva, L.; de Melo, C. G.; Rolim, L. A.; da Silva, R. M. F.; Neto, P. J. R. (2017) Schistosomiasis: drugs used and treatment strategies. *Acta Trop.* 176, 179-187.

(5) Cioli, D.; Pica-Mattoccia, L. (2003) Praziquantel. *Parasitol. Res.* 90 Supp 1, S3-9.

(6) Mader, P.; Rennar, G. A.; Ventura, A. M. P.; Grevelding, C. G.; Schlitzer, M. (2018) Chemotherapy for fighting schistosomiasis: past, present and future. *ChemMedChem* 13, 2374-2389.

(7) Gemma, S.; Federico, S.; Brogi, S.; Brindisi, M.; Butini, S.; Campiani, G. Dealing with schistosomiasis: current drug discovery strategies. In *Ann. Rep.Med. Chem.*, Academic Press: 2019.

(8) Andrews, K. T.; Haque, A.; Jones, M. K. (2012) HDAC inhibitors in parasitic diseases. *Immunol. Cell. Biol.* 90, 66-77.

(9) Hailu, G. S.; Robaa, D.; Forgione, M.; Sippl, W.; Rotili, D.; Mai, A. (2017) Lysine deacetylase inhibitors in parasites: past, present, and future perspectives. *J. Med. Chem.* 60, 4780-4804.

(10) Haberland, M.; Montgomery, R. L.; Olson, E. N. (2009) The many roles of histone deacetylases in development and physiology: implications for disease and therapy. *Nat. Rev. Genet.* 10, 32-42.

(11) Chakrabarti, A.; Oehme, I.; Witt, O.; Oliveira, G.; Sippl, W.; Romier, C.; Pierce, R. J.; Jung, M. (2015) HDAC8: a multifaceted target for therapeutic interventions. *Trends Pharmacol. Sci.* 36, 481-492.

(12) Wolfson, N. A.; Pitcairn, C. A.; Fierke, C. A. (2013) HDAC8 substrates: histones and beyond. *Biopolymers* 99, 112-126.

(13) Gregoretti, I. V.; Lee, Y. M.; Goodson, H. V. (2004) Molecular evolution of the histone deacetylase family: functional implications of phylogenetic analysis. *J. Mol. Biol.* 338, 17-31.

(14) Oger, F.; Dubois, F.; Caby, S.; Noel, C.; Cornette, J.; Bertin, B.; Capron, M.; Pierce, R. J. (2008) The class I histone deacetylases of the platyhelminth parasite *Schistosoma mansoni*. *Biochem. Biophys. Res. Commun.* 377, 1079-1084.

(15) Hu, E.; Chen, Z.; Fredrickson, T.; Zhu, Y.; Kirkpatrick, R.; Zhang, G. F.; Johanson, K.; Sung, C. M.; Liu, R.; Winkler, J. (2000) Cloning and characterization of a novel human class I histone deacetylase that functions as a transcription repressor. *J. Biol. Chem.* 275, 15254-15264.

(16) Marek, M.; Kannan, S.; Hauser, A. T.; Moraes Mourao, M.; Caby, S.; Cura, V.; Stolfa, D. A.; Schmidtkunz, K.; Lancelot, J.; Andrade, L.; Renaud, J. P.; Oliveira, G.; Sippl, W.; Jung, M.; Cavarelli, J.; Pierce, R. J.; Romier, C. (2013) Structural basis for the inhibition of histone deacetylase 8 (HDAC8), a key epigenetic player in the blood fluke *Schistosoma mansoni*. *PLoS Pathog.* 9, e1003645.

(17) Kannan, S.; Melesina, J.; Hauser, A. T.; Chakrabarti, A.; Heimburg, T.; Schmidtkunz, K.; Walter, A.; Marek, M.; Pierce, R. J.; Romier, C.; Jung, M.; Sippl, W. (2014) Discovery of inhibitors of *Schistosoma mansoni* HDAC8 by combining homology modeling, virtual screening, and *in vitro* validation. *J. Chem. Inf. Model.* 54, 3005-3019.

(18) Stolfa, D. A.; Marek, M.; Lancelot, J.; Hauser, A. T.; Walter, A.; Leproult, E.; Melesina, J.; Rumpf, T.; Wurtz, J. M.; Cavarelli, J.; Sippl, W.; Pierce, R. J.; Romier, C.; Jung, M. (2014)

Molecular basis for the antiparasitic activity of a mercaptoacetamide derivative that inhibits histone deacetylase 8 (HDAC8) from the human pathogen *Schistosoma mansoni*. *J. Mol. Biol.* 426, 3442-3453.

(19) Simoben, C. V.; Robaa, D.; Chakrabarti, A.; Schmidtkunz, K.; Marek, M.; Lancelot, J.; Kannan, S.; Melesina, J.; Shaik, T. B.; Pierce, R. J.; Romier, C.; Jung, M.; Sippl, W. (2018) A novel class of *Schistosoma mansoni* Histone Deacetylase 8 (HDAC8) inhibitors identified by structure-based virtual screening and *in vitro* testing. *Molecules* 23.

(20) Bayer, T.; Chakrabarti, A.; Lancelot, J.; Shaik, T. B.; Hausmann, K.; Melesina, J.; Schmidtkunz, K.; Marek, M.; Erdmann, F.; Schmidt, M.; Robaa, D.; Romier, C.; Pierce, R. J.; Jung, M.; Sippl, W. (2018) Synthesis, crystallization studies, and *in vitro* characterization of cinnamic acid derivatives as *Sm*HDAC8 Inhibitors for the treatment of schistosomiasis. *ChemMedChem* 13, 1517-1529.

(21) Heimburg, T.; Chakrabarti, A.; Lancelot, J.; Marek, M.; Melesina, J.; Hauser, A. T.; Shaik, T. B.; Duclaud, S.; Robaa, D.; Erdmann, F.; Schmidt, M.; Romier, C.; Pierce, R. J.; Jung, M.; Sippl, W. (2016) Structure-based design and synthesis of novel inhibitors targeting HDAC8 from *Schistosoma mansoni* for the treatment of schistosomiasis. *J. Med. Chem.* 59, 2423-2435.

(22) Brindisi, M.; Brogi, S.; Relitti, N.; Vallone, A.; Butini, S.; Gemma, S.; Novellino, E.; Colotti, G.; Angiulli, G.; Di Chiaro, F.; Fiorillo, A.; Ilari, A.; Campiani, G. (2015) Structure-based discovery of the first non-covalent inhibitors of *Leishmania major* tryparedoxin peroxidase by high throughput docking. *Sci. Rep.* 5, 9705.

(23) Brindisi, M.; Brogi, S.; Giovani, S.; Gemma, S.; Lamponi, S.; De Luca, F.; Novellino, E.; Campiani, G.; Docquier, J. D.; Butini, S. (2016) Targeting clinically-relevant metallo-beta-lactamases: from high-throughput docking to broad-spectrum inhibitors. *J. Enzyme Inhib. Med. Chem.*, 1-12.

(24) Gasser, A.; Brogi, S.; Urayama, K.; Nishi, T.; Kurose, H.; Tafi, A.; Ribeiro, N.; Desaubry, L.; Nebigil, C. G. Discovery and cardioprotective effects of the first non-Peptide agonists of the G protein-coupled prokineticin receptor-1. *PLoS One* 10, e0121027.

(25) Brindisi, M.; Senger, J.; Cavella, C.; Grillo, A.; Chemi, G.; Gemma, S.; Cucinella, D. M.; Lamponi, S.; Sarno, F.; Iside, C.; Nebbioso, A.; Novellino, E.; Shaik, T. B.; Romier, C.; Herp, D.; Jung, M.; Butini, S.; Campiani, G.; Altucci, L.; Brogi, S. (2018) Novel spiroindoline HDAC inhibitors: synthesis, molecular modelling and biological studies. *Eur. J. Med. Chem.* 157, 127-138.

(26) Paolino, M.; Brindisi, M.; Vallone, A.; Butini, S.; Campiani, G.; Nannicini, C.; Giuliani, G.; Anzini, M.; Lamponi, S.; Giorgi, G.; Sbardella, D.; Ferraris, D. M.; Marini, S.; Coletta, M.; Palucci, I.; Minerva, M.; Delogu, G.; Pepponi, I.; Goletti, D.; Cappelli, A.; Gemma, S.; Brogi, S. (2018) Development of potent inhibitors of the *Mycobacterium tuberculosis* virulence factor Zmp1 and evaluation of their effect on mycobacterial survival inside macrophages. *Chemmedchem* 13, 422-430.

(27) Brindisi, M.; Cavella, C.; Brogi, S.; Nebbioso, A.; Senger, J.; Maramai, S.; Ciotta, A.; Iside, C.; Butini, S.; Lamponi, S.; Novellino, E.; Altucci, L.; Jung, M.; Campiani, G.; Gemma, S. (2016) Phenylpyrrole-based HDAC inhibitors: synthesis, molecular modeling and biological studies. *Future Med. Chem.* 8, 1573-1587.

(28) Glide, version 6.8, Schrödinger, LLC, New York, NY, 2015.

(29) Allwood, D. M.; Blakemore, D. C.; Ley, S. V. (2014) Preparation of unsymmetrical ketones from tosylhydrazones and aromatic aldehydes via formyl C-H bond insertion. *Org. Lett.* 16, 3064-3067.

(30) Karthikeyan, S. V.; Perumal, S.; Shetty, K. A.; Yogeeswari, P.; Sriram, D. (2009) A microwave-assisted facile regioselective Fischer indole synthesis and antitubercular evaluation of novel 2-aryl-3,4-dihydro-2H-thieno[3,2-b]indoles. *Bioorg. Med. Chem. Lett.* 19, 3006-3009.

(31) Lalli, C.; Guidi, A.; Gennari, N.; Altamura, S.; Bresciani, A.; Ruberti, G. (2015) Development and validation of a luminescence-based, medium-throughput assay for drug screening in *Schistosoma mansoni*. *PLoS Negl. Trop. Dis.* 9, e0003484.

(32) Pica-Mattoccia, L.; Cioli, D. (2004) Sex- and stage-related sensitivity of *Schistosoma mansoni* to *in vivo* and *in vitro* praziquantel treatment. *Int. J. Parasitol.* 34, 527-533.

(33) Guidi, A.; Lalli, C.; Gimmelli, R.; Nizi, E.; Andreini, M.; Gennari, N.; Saccoccia, F.; Harper, S.; Bresciani, A.; Ruberti, G. (2017) Discovery by organism based high-throughput screening of new multi-stage compounds affecting *Schistosoma mansoni* viability, egg formation and production. *PLoS Negl. Trop. Dis.* 11, e0005994.

(34) Guidi, A.; Saccoccia, F.; Gennari, N.; Gimmelli, R.; Nizi, E.; Lalli, C.; Paonessa, G.; Papoff, G.; Bresciani, A.; Ruberti, G. (2018) Identification of novel multi-stage histone deacetylase (HDAC) inhibitors that impair *Schistosoma mansoni* viability and egg production. *Parasit. Vectors* 11, 668.

(35) Guidi, A.; Lalli, C.; Perlas, E.; Bolasco, G.; Nibbio, M.; Monteagudo, E.; Bresciani, A.; Ruberti, G. (2016) Discovery and characterization of novel anti-schistosomal properties of the anti-anginal drug, Perhexiline and its impact on *Schistosoma mansoni* male and female reproductive systems. PLoS Negl. Trop. Dis. 10, e000492

(36) Baell, J. B.; Holloway, G. A. (2010) New substructure filters for removal of pan assay interference compounds (PAINS) from screening libraries and for their exclusion in bioassays. *J. Med. Chem.* 53, 2719-2740.

(37) Lagorce, D.; Sperandio, O.; Baell, J. B.; Miteva, M. A.; Villoutreix, B. O. (2015) FAF-Drugs3: a web server for compound property calculation and chemical library design. *Nucleic Acids Res.* 43, W200-207.

(38) Alam, N.; Zimmerman, L.; Wolfson, N. A.; Joseph, C. G.; Fierke, C. A.; Schueler-Furman, O. (2016) Structure-based identification of HDAC8 non-histone substrates. *Structure* 24, 458-468.

(39) Olson, D. E.; Udeshi, N. D.; Wolfson, N. A.; Pitcairn, C. A.; Sullivan, E. D.; Jaffe, J. D.; Svinkina, T.; Natoli, T.; Lu, X.; Paulk, J.; McCarren, P.; Wagner, F. F.; Barker, D.; Howe, E.; Lazzaro, F.; Gale, J. P.; Zhang, Y. L.; Subramanian, A.; Fierke, C. A.; Carr, S. A.; Holson, E. B. (2014) An unbiased approach to identify endogenous substrates of histone deacetylase 8. *ACS Chem. Biol.* 9, 2210-2216.

(40) Hong, Y.; Cao, X.; Han, Q.; Yuan, C.; Zhang, M.; Han, Y.; Zhu, C.; Lin, T.; Lu, K.; Li, H.; Fu, Z.; Lin, J. (2016) Proteome-wide analysis of lysine acetylation in adult *Schistosoma japonicum* worm. *J. Proteomics* 148, 202-212.

(41) Maestro. *Maestro*, 9.2; Schrödinger, LLC: New York, NY, 2011, 2011.

(42) MacroModel. version 10.9, Schrödinger, LLC, New York, NY, 2015.

(43) Jorgensen, W. L.; Maxwell, D. S.; TiradoRives, J. (1996) Development and testing of the OPLS all-atom force field on conformational energetics and properties of organic liquids. *J. Am. Chem. Soc.* 118, 11225-11236.

(44) LigPrep. version 3.5, Schrödinger, LLC, New York, NY, 2015.

(45) Friesner, R. A.; Banks, J. L.; Murphy, R. B.; Halgren, T. A.; Klicic, J. J.; Mainz, D. T.; Repasky, M. P.; Knoll, E. H.; Shelley, M.; Perry, J. K.; Shaw, D. E.; Francis, P.; Shenkin, P. S. (2004) Glide: a new approach for rapid, accurate docking and scoring. 1. Method and assessment of docking accuracy. *J. Med. Chem.* 47, 1739-1749.

(46) Maestro. version 10.3, Schrödinger, LLC, New York, NY, 2015.

(47) Marek, M.; Shaik, T. B.; Duclaud, S.; Pierce, R. J.; Romier, C. (2016) Large-scale overproduction and purification of recombinant Histone Deacetylase 8 (HDAC8) from the human-pathogenic flatworm *Schistosoma mansoni*. *Methods Mol. Biol.* 1436, 109-118.

(48) Marek, M.; Shaik, T. B.; Heimburg, T.; Chakrabarti, A.; Lancelot, J.; Ramos-Morales, E.; Da Veiga, C.; Kalinin, D.; Melesina, J.; Robaa, D.; Schmidtkunz, K.; Suzuki, T.; Holl, R.; Ennifar, E.; Pierce, R. J.; Jung, M.; Sippl, W.; Romier, C. (2018) Characterization of Histone Deacetylase 8 (HDAC8) selective inhibition reveals specific active site structural and functional determinants. *J. Med. Chem.* 61, 10000-10016.

(49) Heltweg, B.; Dequiedt, F.; Verdin, E.; Jung, M. (2003) Nonisotopic substrate for assaying both human zinc and NAD^+-dependent histone deacetylases. *Anal. Biochem.* 319, 42-48.

(50) Wegener, D.; Wirsching, F.; Riester, D.; Schwienhorst, A. (2003) A fluorogenic histone deacetylase assay well suited for high-throughput activity screening. *Chem. Biol.* 10, 61-68.

(51) Heltweg, B.; Trapp, J.; Jung, M. (2005) *In vitro* assays for the determination of histone deacetylase activity. *Methods* 36, 332-337.

(52) Dubois, F.; Caby, S.; Oger, F.; Cosseau, C.; Capron, M.; Grunau, C.; Dissous, C.; Pierce, R. J. (2009) Histone deacetylase inhibitors induce apoptosis, histone hyperacetylation and up-regulation of gene transcription in *Schistosoma mansoni*. *Mol. Biochem. Parasitol.* 168, 7-15.

(53) Brink, L. H.; McLaren, D. J.; Smithers, S. R. (1977) *Schistosoma mansoni:* a comparative study of artificially transformed schistosomula and schistosomula recovered after cercarial penetration of isolated skin *Parasitology* 74, 73-86.

(54) Protasio, A. V.; Dunne, D. W.; Berriman, M. (2013) Comparative study of transcriptome profiles of mechanical- and skin-transformed *Schistosoma mansoni* schistosomula. *PLoS Negl. Trop. Dis.* 7, e2091.

FIGURE LEGENDS

Figure 1. Structures of currently used anti-schistosoma drug praziquantel (1), of two selected inhibitors of SmHDAC8 reported in the literature (2, 3), and general structures of compounds investigated in the present work (4-12).

Figure 2. Synthetic pathways for the preparation of compounds **6-11**. (A) a.1-Methyl-4-piperidone, MeOH, 25 °C; b. 3-Cl or 4-Cl-benzaldehyde, Cs_2CO_3, dioxane, 110 °C; c. $PhNHNH_2$, H_2SO_4, dioxane, 60 °C; d. $NaBH_4$, MeOH, 50 °C; e. methyl 4-formylbenzoate, AcOH, $NaBH_3CN$, EtOH, 70 °C; f. $NH_2OHxHCl$, KOH, DCM/MeOH, 25 °C. (B) a. mercaptoacetic acid, Et_3N, dioxane, reflux; b. NaOAc, Ac_2O, reflux, then H_2SO_4; c. 4-Cl or 4-F-$PhNHNH_2$, H_2SO_4, EtOH, MW (150 W); d. KOtBu, KI, 4-(bromomethyl)benzoate, DMF, 80 °C; e. $NH_2OHxHCl$, KOH, DCM/MeOH, 25 °C; f.KOtBu, KI, methyl 5-(bromomethyl)thiophene-2-carboxylate, DMF, 80 °C. (C) a. acetone, MeOH, 25 °C; b. 4-methoxyphenylhydrazine, H_2SO_4, dioxane, 60 °C; c. 3-pyridylaldehyde, Cs_2CO_3, dioxane, 110 °C; d. 4-OMe$PhNHNH_2$, H_2SO_4, dioxane, 60 °C; e. $NaBH_4$, MeOH, 50 °C; e. methyl 4-formylbenzoate, AcOH, $NaBH_3CN$, EtOH, 70 °C; f. $NH_2OHxHCl$, KOH, DCM/MeOH, 25 °C.

Figure 3. ATP quantitation and MTT assays to assess schistosomula survival and mammalian cytotoxicity with selected compounds. (A) The calculated LC_{50} and 95% confidence interval (CI) values for the indicated compounds are shown. (B) Dose-response curves of the hit compounds (**4**, **6**, **8**, **11**) on schistosomula. Schistosomula (150-200/well) were incubated with serial dilutions of the indicated compounds, 5 wells at each concentration. The % ATP reduction (death of schistosomula) plotted on the y-axis revealed in 72 h incubation were normalized based on 50 μM GA-treated control (0% survival) and DMSO treated schistosomula (100% survival). Each point represents the average and SEM. (C) Effects of selected schistosomicidal compounds on cell viability. NIH-3T3 mammalian

cells were treated with serial diluitions of the compounds, MTT assays were performed. The IC_{50} ± SEM values of three independent experiments are shown.

Figure 4. Adult schistosome pairs viability assays. DMSO (vehicle) (black up-poiting triangle) was used as negative control (100% viability) and the indicated compounds were assayed at 20 μM (open circle) and 50 μM (gray bottom-pointing triangle). Viability is reported as residual percentage with respect to the DMSO-treated samples. Each point represents the average ± SEM of three independent experiments.

Figure 5. (A) Egg laying impairment. Histograms showing the total egg counts normalized to worm pairs treated for 72 h with sub-lethal concentrations of the indicated compounds: **6** and **7** (10 μM), **8** (20 μM), **9** (30 μM), **10** (5 μM). DMSO-treated worms were used as reference. Each point represents the average ± SEM of at least three independent experiments. The levels of statistical significance are indicated above bars; *P <0.05, **P <0.01 or ***P <0.001, Student's t test. (B) Representative microscopy images of *S. mansoni* eggs laid *in vitro* by worm pairs treated with vehicle or the selected compounds at sub-lethal concentrations as in (A) for 72 h. Abbreviations stand for: e, egg; de, deformed egg; ef, egg fragments; vc, vitellocyte; sp, sperm cells; oc, oocyte. In all experiments (panels A, B), vehicle-treated parasites received the same amount of DMSO (in volume) as the compound-treated ones. Scale-bar: 200 μm.

Figure 6. Confocal microscopy of carmine red-stained adult worm couples treated with DMSO, compounds 6 (10 μM) and 8 (20 μM). The images are representative of five worm pairs. The ovary, ootype, vitellarium, testis and parenchymal tissue are shown. Abbreviations stand for: io, immature oocytes; mo, mature oocytes; ut, uterus; ot, ootype; sv, seminal vesicle; vt, vitellarium; star, egg; white triangle, black spot in oocytes; red triangle, unstained, hole-like areas within vitellarium; red arrows, cell degeneration; asterisk, sperm cells; white arrows, unstained, hole-like areas buried into parenchyma. Scale-bar: 50 μm.

Figure 7. Male juvenile worm's viability curves. For each compound, DMSO (balsck up-pointing triangle), 20 μM (open circles) and 50 μM (gray down-pointing triangle) treatment are reported in the graph as % of viability. Each point represents the average ± SEM of three independent experiments.

Figure 8. HDAC activity inhibitory potency (IC_{50}, μM ±SEM) of compounds 6-11 against recombinant form of human and *S. mansoni* HDAC8 enzymes (panels A and B respectively), and human HDAC1 (panel C). The reference compound 3 was tested under the same experimental conditions and reported for comparison in panels A and B. The IC50 HDAC1 activity inhibitory potency (6.3 ± 2.1 μM) has been previously reported. [21]

Figure 9. Docked poses for compounds 6 (R-enantiomer pose represented as deep teal sticks, panel A; S-enantiomer pose represented as blue sticks, panel B) and 10 (R-enantiomer pose represented as lime green sticks, panel C; S-enantiomer pose represented as green sticks, panel D) into SmHDAC8 enzyme (light pink cartoon PDB ID: 4BZ7). The residues of the active site are represented as line and the Zn^{2+} is represented as a gray sphere. H-bonds are represented as yellow dotted lines, while red and blue dotted lines represent the metal coordination bonds. Figures were prepared using PyMOL (The PyMOL Molecular Graphics System, v1.8.4.0, Schrödinger LLC, New York, 2015).

Figure 10. Effects of selected compounds on histones acetylation. Representative immunoblot of the histone-enriched protein fractions extracted from *S. mansoni* adult worm pairs incubated with anti-acetylated lysine antibody (acetylated-K) or anti-tubulin. Worm pairs were treated for 72 h with 20 μM of the indicated compounds (sub-lethal dose). DMSO (vehicle) and 1 μM of the HDAC pan-inhibitor, TSA were used as negative and positive controls, respectively.

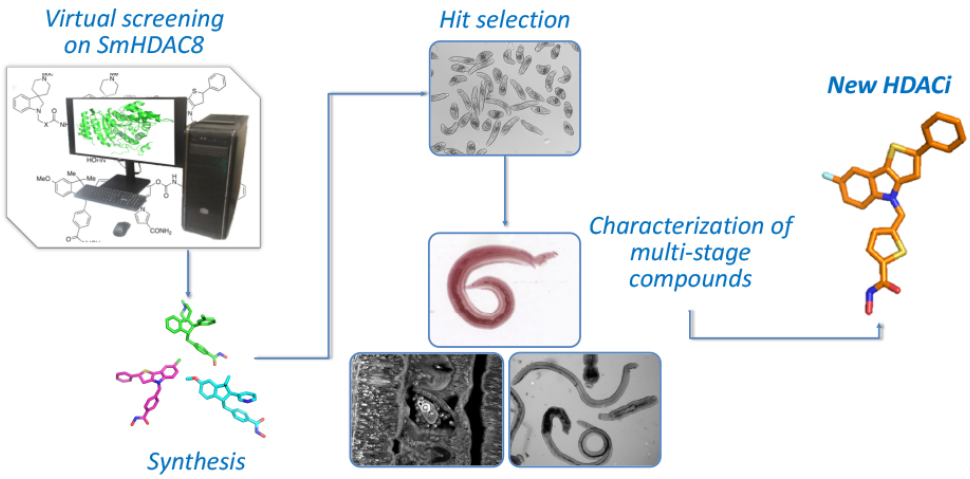

"For Table of Contents Use Only"

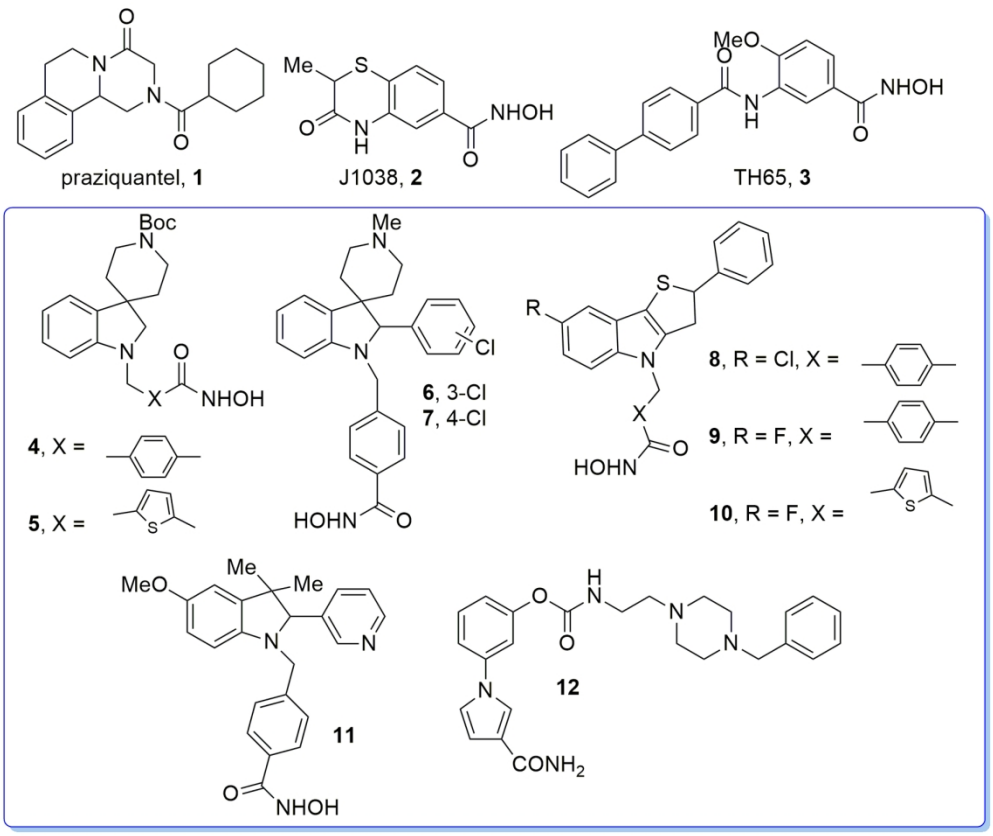

Figure 1. Structures of currently used anti-schistosoma drug praziquantel (1), of two selected inhibitors of SmHDAC8 reported in the literature (2, 3), and general structures of compounds investigated in the present work (4-12).

161x134mm (300 x 300 DPI)

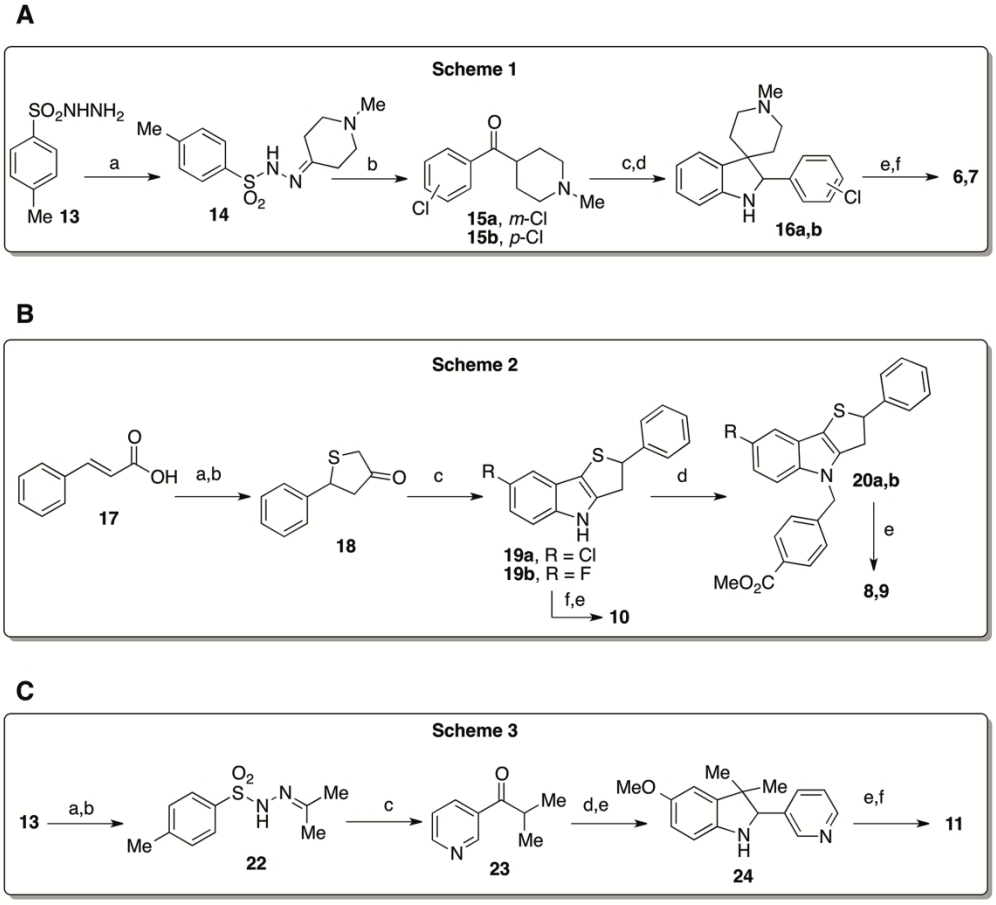

Figure 2. Synthetic pathways for the preparation of compounds 6-11. (A) a.1-Methyl-4-piperidone, MeOH, 25 °C; b. 3-Cl or 4-Cl-benzaldehyde, Cs2CO3, dioxane, 110 °C; c. PhNHNH2, H2SO4, dioxane, 60 °C; d. NaBH4, MeOH, 50 °C; e. methyl 4-formylbenzoate, AcOH, NaBH3CN, EtOH, 70 °C; f. NH2OHxHCl, KOH, DCM/MeOH, 25 °C. (B) a. mercaptoacetic acid, Et3N, dioxane, reflux; b. NaOAc, Ac2O, reflux, then H2SO4; c. 4-Cl or 4-F-PhNHNH2, H2SO4, EtOH, MW (150 W); d. KOtBu, KI, 4-(bromomethyl)benzoate, DMF, 80 °C; e. NH2OHxHCl, KOH, DCM/MeOH, 25 °C; f.KOtBu, KI, methyl 5-(bromomethyl)thiophene-2-carboxylate, DMF, 80 °C. (C) a. acetone, MeOH, 25 °C; b. 4-methoxyphenylhydrazine, H2SO4, dioxane, 60 °C; c. 3-pyridylaldehyde, Cs2CO3, dioxane, 110 °C; d. 4-OMePhNHNH2, H2SO4, dioxane, 60 °C; e. NaBH4, MeOH, 50 °C; e. methyl 4-formylbenzoate, AcOH, NaBH3CN, EtOH, 70 °C; f. NH2OHxHCl, KOH, DCM/MeOH, 25 °C.

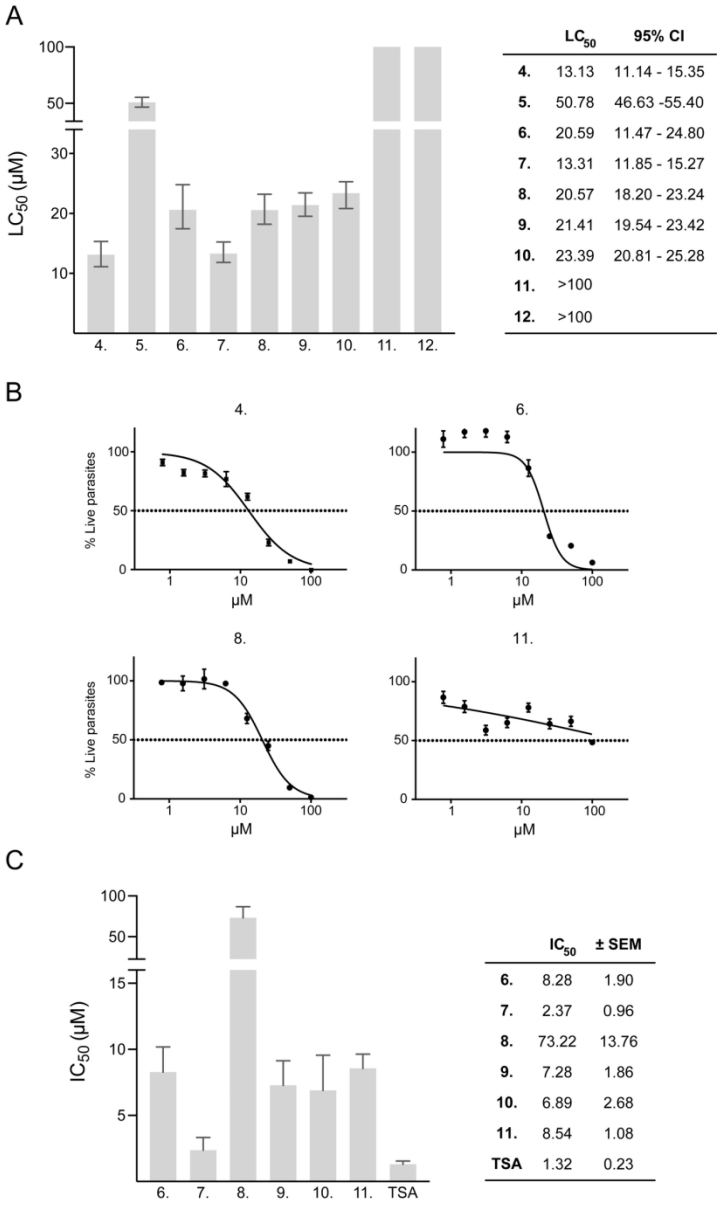

Figure 3. ATP quantitation and MTT assays to assess schistosomula survival and mammalian cytotoxicity with selected compounds. (A) The calculated LC50 and 95% confidence interval (CI) values for the indicated compounds are shown. (B) Dose-response curves of the hit compounds (4, 6, 8, 11) on schistosomula. Schistosomula (150-200/well) were incubated with serial dilutions of the indicated compounds, 5 wells at each concentration. The % ATP reduction (death of schistosomula) plotted on the y-axis revealed in 72 h incubation were normalized based on 50 μM GA-treated control (0% survival) and DMSO treated schistosomula (100% survival). Each point represents the average and SEM. (C) Effects of selected schistosomicidal compounds on cell viability. MTT assays on NIH-3T3 mammalian cells treated with serial dilutions of the selected compounds: the IC50 ± SEM values of three independent experiments are shown.

113x191mm (300 x 300 DPI)

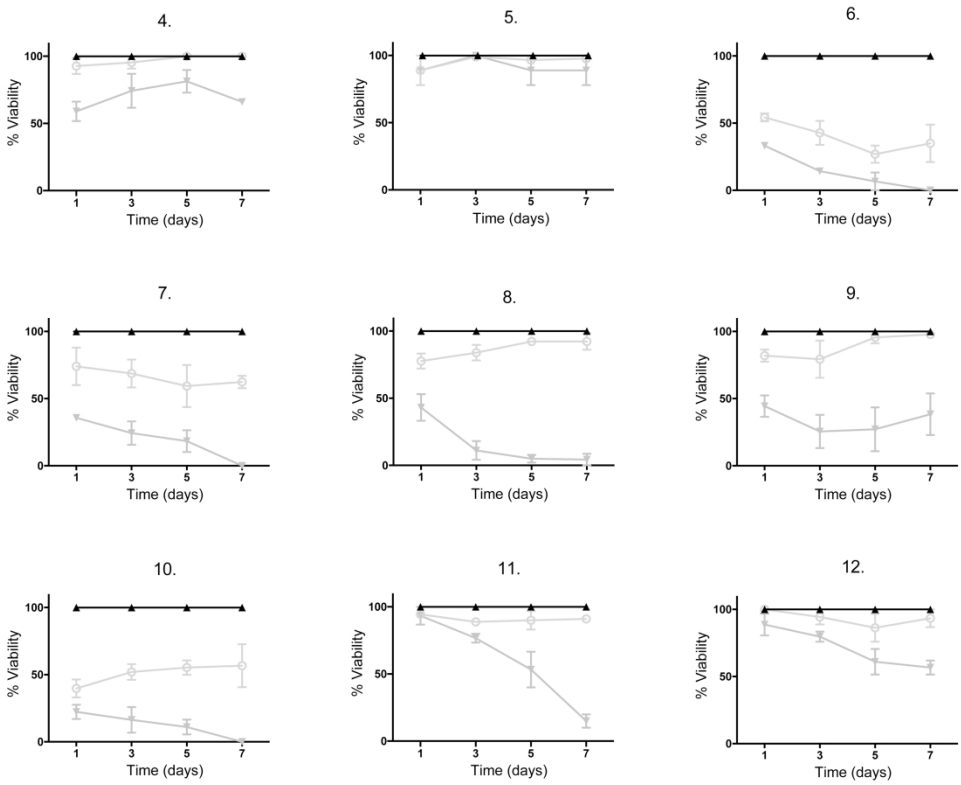

Figure 4. Adult schistosome pairs viability assays. DMSO (vehicle) (black up-pointing triangle) was used as negative (100% viability) control and the indicated compounds were assayed at 20 μM (open circle) and 50 μM (gray down-pointing triangle). Viability is reported as residual percentage with respect to the DMSO-treated samples. Each point represents the average ± SEM of three independent experiments.

144x114mm (600 x 600 DPI)

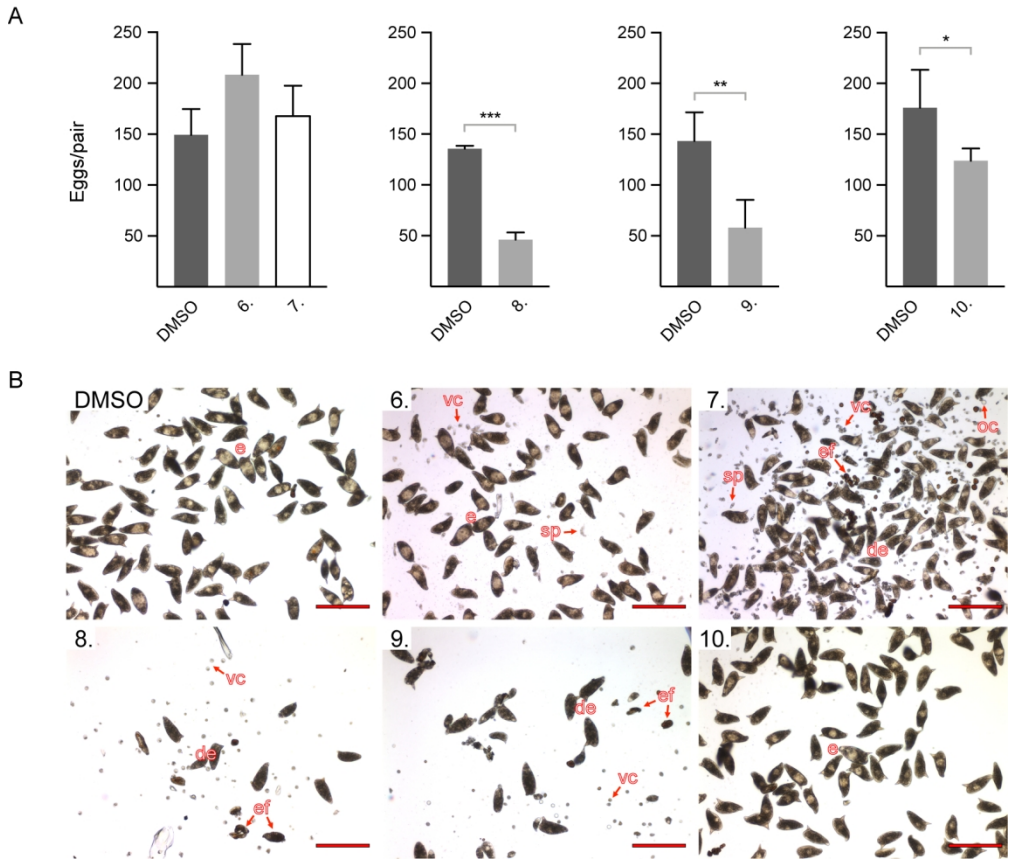

Figure 5. (A) Egg laying impairment. Histograms showing the total egg counts normalized to worm pairs treated for 72 h with sub-lethal concentrations of the indicated compounds: 6 and 7 (10 μM), 8 (20 μM), 9 (30 μM), 10 (5 μM). DMSO-treated worms were used as reference. Each point represents the average ± SEM of at least three independent experiments. The levels of statistical significance are indicated above bars; *P <0.05, **P <0.01 or ***P <0.001, Student's t test. (B) Representative microscopy images of S. mansoni eggs laid in vitro by worm pairs treated with vehicle or the selected compounds at sub-lethal concentrations as in (A) for 72 h. Abbreviations stand for: e, egg; de, deformed egg; ef, egg fragment; vc, vitellocyte; sp, spermatozoa; oc, oocyte. In all experiments (panels A, B), vehicle-treated parasites received the same amount of DMSO (in volume) as the compound-treated ones. Scale-bar: 200 μm.

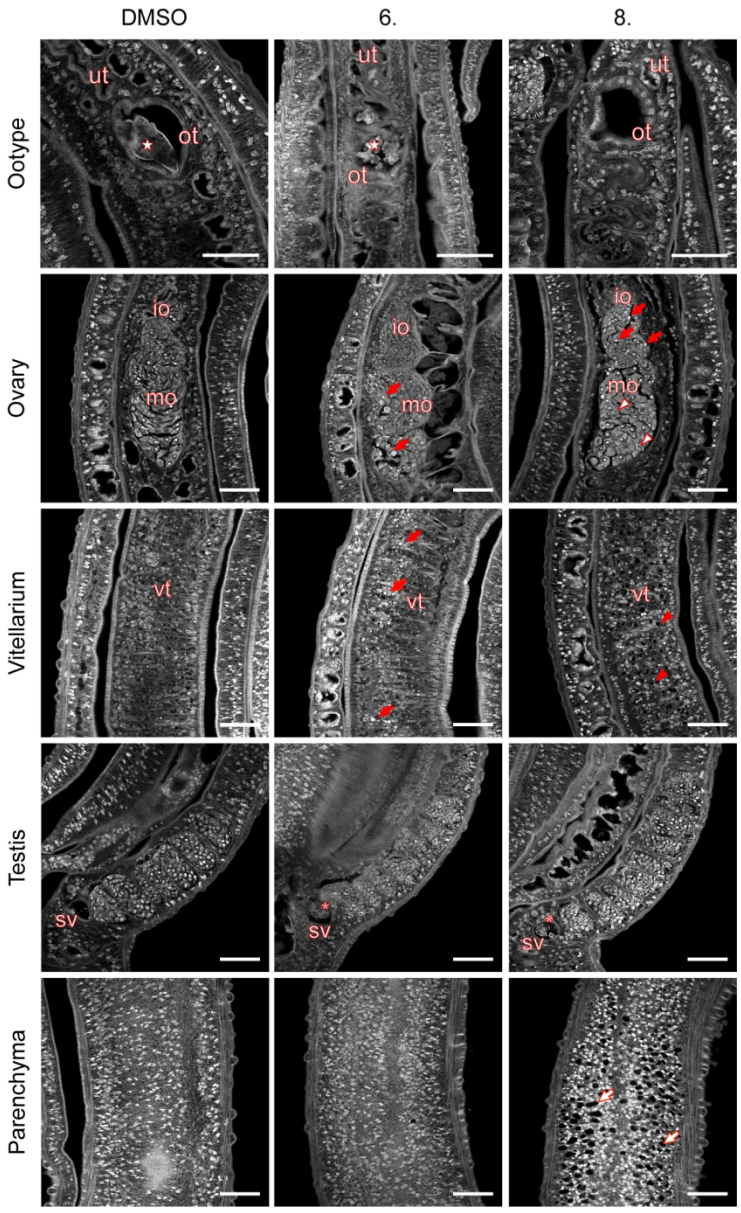

Figure 6. Confocal microscopy of carmine red-stained adult worm couples treated with DMSO, compounds 6 (10 μM) and 8 (20 μM). The images are representative of five worm pairs. The ovary, ootype, vitellarium, testis and parenchymal tissue are shown. Abbreviations stand for: io, immature oocytes; mo, mature oocytes; ut, uterus; ot, ootype; sv, seminal vesicle; vt, vitellarium; star, egg; white triangle, black spot in oocytes; red triangle, unstained, hole-like areas within vitellarium; red arrow; cell degeneration; asterisk, sperm cells; white arrow, unstained, hole-like areas buried into parenchyma. Scale-bar: 50 μm.

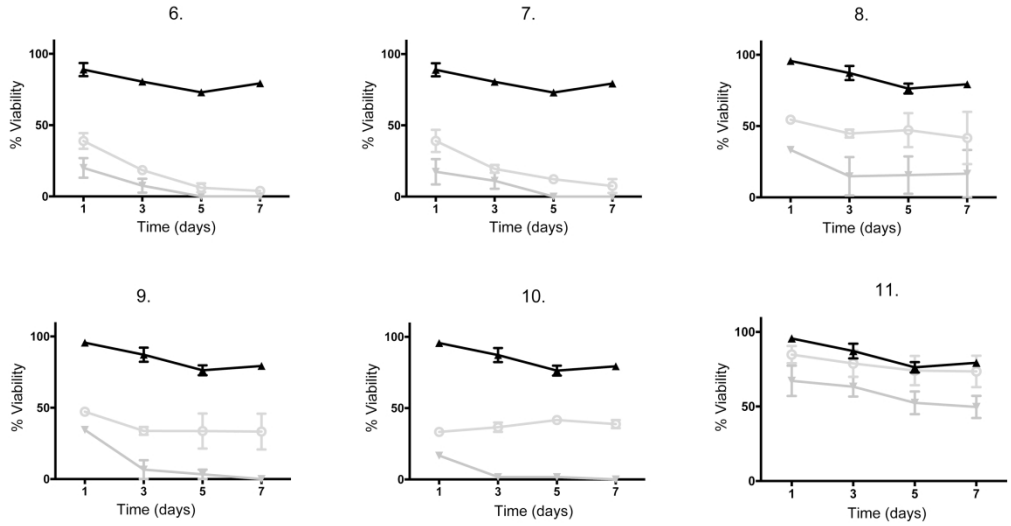

Figure 7. Male juvenile worm's viability curves. For each compound, DMSO (black up-pointing triangle), 20 μM (open circle) and 50 μM (gray down-pointing triangle) treatment are reported in the graph as % of viability. Each point represents the average ± SEM of three independent experiments.

141x73mm (600 x 600 DPI)

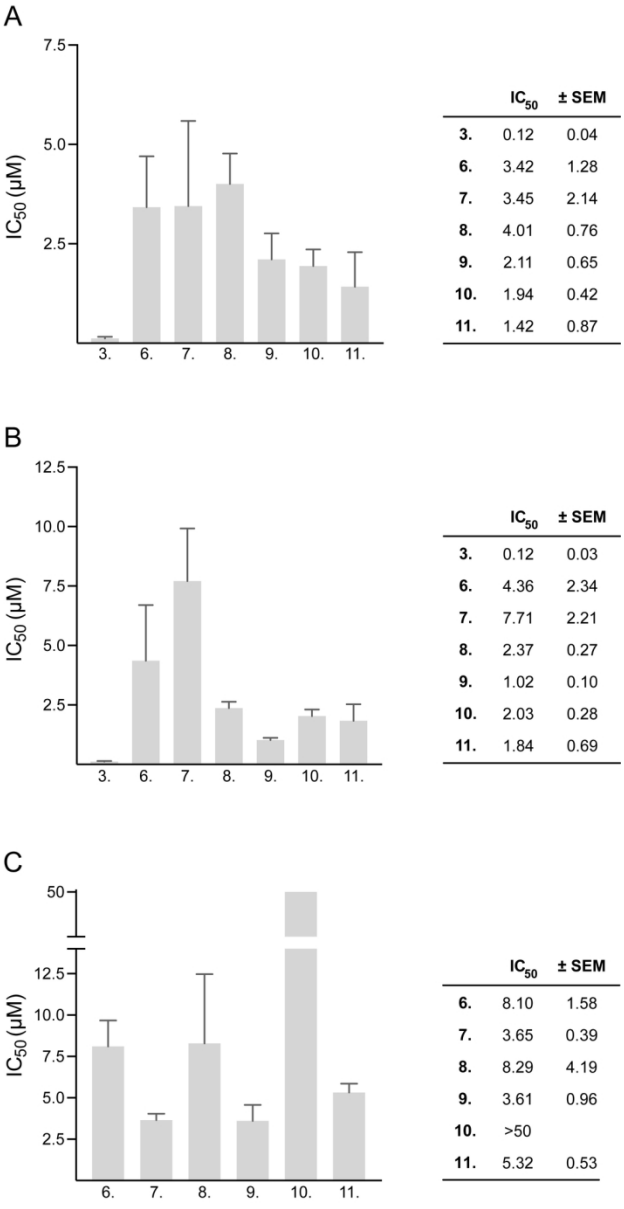

	IC_{50}	± SEM
3.	0.12	0.04
6.	3.42	1.28
7.	3.45	2.14
8.	4.01	0.76
9.	2.11	0.65
10.	1.94	0.42
11.	1.42	0.87

	IC_{50}	± SEM
3.	0.12	0.03
6.	4.36	2.34
7.	7.71	2.21
8.	2.37	0.27
9.	1.02	0.10
10.	2.03	0.28
11.	1.84	0.69

	IC_{50}	± SEM
6.	8.10	1.58
7.	3.65	0.39
8.	8.29	4.19
9.	3.61	0.96
10.	>50	
11.	5.32	0.53

Figure 8. HDAC activity inhibitory potency (IC50, μM ±SEM) of compounds 6-11 against recombinant form of human and S. mansoni HDAC8 enzymes (panels A and B respectively), and human HDAC1 (panel C). The reference compound 3 was tested under the same experimental conditions and reported for comparison in panels A and B. The IC50 HDAC1 activity inhibitory potency (6.3 ± 2.1 μM) has been previously reported. 21

94x183mm (300 x 300 DPI)

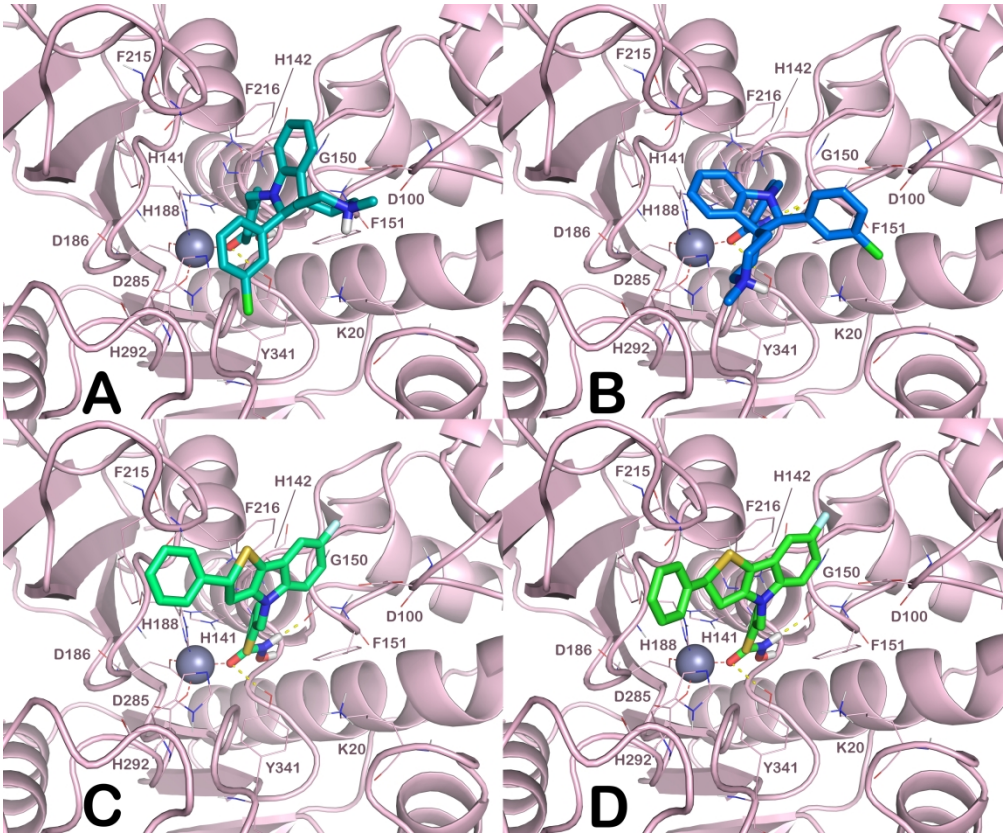

Figure 9. Docked poses for compounds 6 (R-enantiomer pose represented as deep teal sticks, panel A; S-enantiomer pose represented as blue sticks, panel B) and 10 (R-enantiomer pose represented as lime green sticks, panel C; S-enantiomer pose represented as green sticks, panel D) into SmHDAC8 enzyme (light pink cartoon PDB ID: 4BZ7). The residues of the active site are represented as line and the Zn2+ is represented as a gray sphere. H-bonds are represented as yellow dotted lines, while red and blue dotted lines represent the metal coordination bonds. Figures were prepared using PyMOL (The PyMOL Molecular Graphics System, v1.8.4.0, Schrödinger LLC, New York, 2015).

169x140mm (600 x 600 DPI)

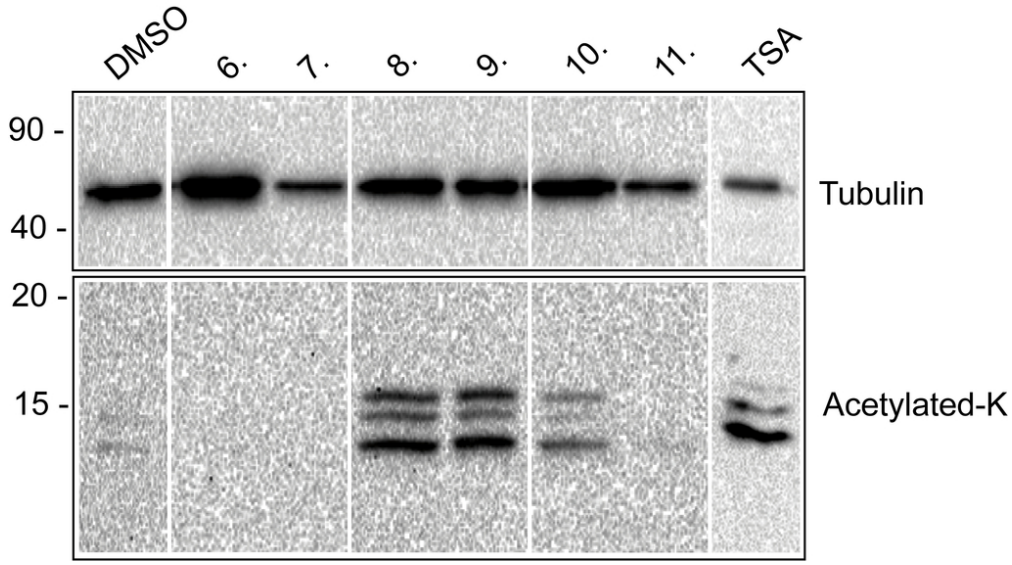

Figure 10. Effects of selected compounds on histones acetylation. Representative immunoblot of the histone-enriched protein fractions extracted from S. mansoni adult worm pairs incubated with anti-acetylated lysine antibody (acetylated-K) or anti-tubulin. Worm pairs were treated for 72 h with 20 μM of the indicated compounds (sub-lethal dose). DMSO (vehicle) and 1 μM of the HDAC pan-inhibitor, TSA were used as negative and positive controls, respectively.

86x48mm (300 x 300 DPI)